24th COBEM - 2017

24th ABCM International Congress of Mechanical Engineering
December 3-8, 2017, Curitiba, PR, Brazil

COBEM-2017-2168
MATHEMATICAL MODELLING OF MACROSEGREGATION IN INGOT CASTING

Milton Assunção
Department of Applied Mathematics and Statistics, Institute of Mathematical and Computer Sciences, University of São Paulo. São Carlos, São Paulo, Brazil
assuncao@icmc.usp.br

Michael Vynnycky
Division of Processes, Department of Materials Science and Engineering, KTH Royal Institute of Technology. Stockholm, Sweden
michaelv@kth.se

Abstract. *The occurrence of macrosegregation in alloys produced by ingot casting can adversely affect the quality of the final product. Macrosegregation can be described as a severe variation on the macroscopic scale of the chemical species that compose the alloy, and the ability of computational simulations to predict such defects remains far from perfect. Therefore, this research focuses on the development of a two-dimensional mathematical model that - through computational simulations - could be applied to study and predict the formation of macrosegregation in the ingot casting of binary alloys. Once accomplished, this work can establish the framework to new studies that will tackle more advanced problems, e.g., for actual ingot geometries, three-dimensional models and industrially-important ternary alloys.*

Keywords: *mathematical modelling, ingot casting, solidification, macrosegregation*

1. INTRODUCTION

Ingots are single blocks of metal, typically steel and weighing from a few kilos to a few tons, which are created by means of a casting procedure where molten metal is fed into cooling moulds. There, it is left until it completely solidifies. The applications for ingot casting include, according to P. Patil and Balasubramanian (2015), forging die blocks, heavy equipment, ship engine parts, pressure vessel parts, oil well equipment, turbine rotors, valve bodies, auto shafts, etc.

To model the solidification process with the aid of computational simulations may help to reduce the cost of production, and prevent defects such as macrosegregation. These are basically differences in concentration over a length scale of the ingot itself. They are defects whose formation an severity is very sensitive to the casting procedure and the ingot size (Pickering, 2013).

It is understood that the causes of macrosegregation are related, according to (Flemings, 1974), to the movement of liquid and solid inside the mushy zone. Highly segregated phases (with great differences in concentration) can be found in this region during the solidification process; it is the physical displacement of these phases that induces macrosegregation. Among other kinds of macrosegregation, the A-segregation, as stated in (Fredriksson and Åkerlind, 2006), is caused by natural convection in the molten metal, which in turn is driven by a density gradient. This kind of segregation importantly concerns high pressure vessels manufacturers: the vessels are built through the removal of the internal portion of a steel ingot, followed by the installation of metallic parts on its interior by welding. However, the procedure's integrity is worsened if the weld matches with A-segregated regions, which are characteristically stiffer, but have less tenacity (Maidorn and Blind, 1985). If exposed during forging or rolling operations to which this product is submitted, the whole ingot must sometimes be discarded.

2. COMPUTATIONAL PROCEDURE

One simple approach to model macrosegregation is to formulate a set of equations valid on all the regions mentioned before - the solid, liquid and mush; this is categorized as a single-domain approach. Another approach is to develop equations for each one of the domains separately. The advantage of the former over the latter is that there is no need to track the solid/mush and mush/liquid moving boundaries that could develop with complex shapes as the simulation proceeds. This simplication can be done following (Amberg, 1991), by including terms in the original equations to keep a balance between solid and liquid fractions. In the single-domain approach, it is then possible to write down the model considering the fundamental laws of mass, momentum, and energy conservation, plus thermodynamic relations valid for

phase changes, as follows.

2.1 Mass and momentum conservation

Assuming the solid and liquid phase densities to be equal, the velocity field may be obtained from a momentum balance valid in all three regions as

$$\nabla \cdot (\chi \mathbf{u}) = 0, \tag{1}$$

$$\rho_0 \left(\frac{\partial \mathbf{u}}{\partial t} + \mathbf{u} \cdot \nabla \mathbf{u} \right) - \mu \nabla^2 \mathbf{u} = -\nabla p - \rho \mathbf{g} - \frac{\mu}{H(\chi)} \chi \mathbf{u}. \tag{2}$$

In Eq. (2), ρ_0 is the density in [kg/m^3] and refers to initial liquid state, while the local density ρ can be written as a function of temperature and concentration measured in a certain control volume, such relation may be presented as soon as the solute concentration is adequately defined. The vector $\mathbf{u}$ is the velocity, written in [m/s]; moreover, the velocity in the mush must be understood as an average among velocities inside porous domain. μ is the dynamic viscosity in [N s/m^2], the pressure p is given in [N/m^2], $\mathbf{g}$ stands for gravity (9.8 m/s^2), χ represents the liquid fraction, which means the unsolidified portion inside a control volume, in a range from 0 (solid) to 1 (liquid).

Here, the permeability $H(\chi)$ measures, as stated by (Fredriksson and Åkerlind, 2006), the ability of the liquid to penetrate through the dendrites of a region where the solidification process has begun and can be given by expressions presented in (West, 1985), where the permeability is described as a function of liquid fraction in accordance to the applicability to the mush zone of metallic alloys, such expressions are given in Eq. (3) and behaved well when compared to experimental data obtained by the author, as exibited in Fig.1.

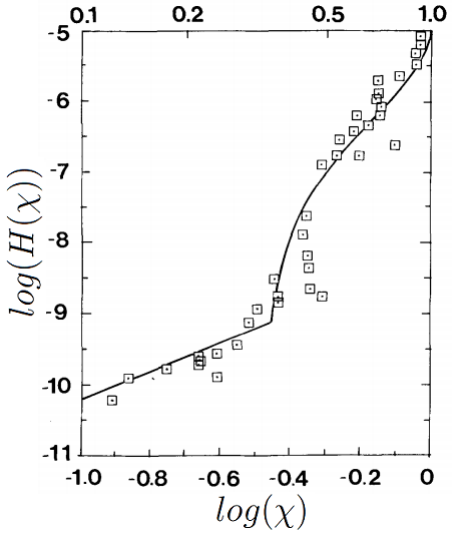

Figure 1: Permeability vs liquid fraction, squares represent the experimental data and the solid line is the function used to predict the permeability. Adapted from (West, 1985)

It can be observed that while the solidification process did not start in a certain region, i.e. ($\chi = 1$), then the last term on righ-hand side of Eq. (2) vanishes, leaving the usual Navier-Stokes equation. Once the solidification has started, the term gains importance in the equation, whilst the velocity tends to zero making the terms on the left-hand side of the equation negligible.

$$H(\chi) = Y_1 K_1 + Y_2 K_2, \tag{3}$$

where $K_1 = \chi^2$, and

$$K_2 = \begin{cases} 0, & \text{if} \quad \chi < \frac{1}{3}, \\ (1-\chi)^{(2/3)} \left(3 + \dfrac{4}{1-\chi} - 3\sqrt{\dfrac{8}{1-\chi} - 3} \right), & \text{if} \quad \chi \geq \frac{1}{3}. \end{cases} \tag{4}$$

The parameters Y_1 and Y_2 are constants obtained by experiments carried in (Piwonka and Flemings, 1966), in which the values were found to be $Y_1 = 6.4 \times 10^{-9}$cm^2 and $Y_2 = 8.8 \times 10^{-7}$cm^2.

2.2 Heat equation

The temperature in each control volume can be obtained from the basic heat equation in terms of a unique temperature, T, valid for liquid, mushy and solid regions:

$$\rho_0 C_\mathrm{p}\left(\frac{\partial T}{\partial t}+\chi\mathbf{u}\cdot\nabla T\right)=\nabla\cdot(\kappa\nabla T)-L_\mathrm{at}\frac{\partial\chi}{\partial t} \tag{5}$$

where C_p is the specific heat in [J/(kg K)], κ is the thermal conductivity in [W/(m K)], while L_at represents the latent heat of fusion [J/kg]. κ can be written as

$$\kappa=\chi\kappa_l+(1-\chi)\kappa_s, \tag{6}$$

which constitutes a linear interpolation between the thermal conductivities of the solid and liquid phases.

The boundary conditions considered in problems of this nature may vary depending on the authors approach. Here, the classical Fourier law stated in Eq. (7) was adopted. It poses the heat flux q[W/m^2] as proportional to the magnitude of the temperature gradient and opposite to it in sign, with κ as the constant of proportionality. (Lienhard IV and Lienhard V, 2017)

$$-\kappa\frac{\partial T}{\partial\mathbf{n}}=q, \tag{7}$$

where $\mathbf{n}$ is the vector normal to the boundary to which this boundary condition is applied. This configures a Neumman boundary condition used to define the heat exchange of the ingot surface with its surroundings.

2.3 Solute conservation

The mass conservation for the solute may be obtained, according to (Amberg, 1991), as

$$\frac{\partial c_\mathrm{m}}{\partial t}+\nabla\cdot(\mathbf{u}\chi c_\mathrm{l})=D\nabla^2 c_\mathrm{m}, \tag{8}$$

with diffusion coefficient D, where c_l represents the local solute concentration in the metallic alloy, c_m is the mixture solute concentration obtained as a balance between the concentrations for liquid and solid phase, c_l and c_s respectively, in the form

$$c_\mathrm{m}=\chi c_\mathrm{l}+(1-\chi)c_\mathrm{s}. \tag{9}$$

In addition, c_s and c_l are related to each other from the phase diagram (for the Fe-c system in the case of steel with no additional elements) by $c_\mathrm{s}=K_\mathrm{p}c_\mathrm{l}$, with K_p as the partition coefficient.

The boundary condition imposed here was the zero flux for the whole domain boundary, which appropriately means that there is no transport of solute across the walls.

Now, it is possible to define an appropriate way to write the density ρ like a function of temperature and concentration as

$$\rho=\rho_0(1+\alpha'(T-T_0)+fc_\mathrm{l}) \tag{10}$$

Where T_0 is the melting temperature for pure iron (0% carbon), $\alpha'=\dfrac{d}{e+100c_\mathrm{l}}$, and the numerical parameters d, e, f are given by (Olsson, 1980) and are presented in Tab. 1.

2.4 Liquid fraction

Observe that there is no explicit partial differential equation for χ; instead, its local value in the mushy region is given implicitly by the relation $T=T_\mathrm{l}(c_\mathrm{l})$,where T_l is the liquidus temperature, determined as a function of c_l from the phase diagram. An artificial way to ensure that this relation is satisfied is to introduce the equation

$$\frac{\partial\chi}{\partial t}=\frac{1}{\epsilon}(T-T_\mathrm{l}(c_\mathrm{l})), \tag{11}$$

Table 1: Physical parameters adopted in the simulations

Variable	Value	Units
C_p	753	J kg^{-1} K^{-1}
D	1e-9	m ^{2} s^{-1}
d	-4.2e-4	1
e	0.55	1
ϵ	1e-6	1
f	-8	1
g	9.8	m s^{-2}
Γ	7800	°C wt^{-1}
κ_l	30	W m^{-1} K^{-1}
K_p	0.42	1
κ_s	60	W m^{-1} K^{-1}
L	0.1	m
L_{at}	2.72e5	J kg^{-1}
μ	6.94e-3	N s m^{-2}
ρ_0	6940	kg m^{-3}
q	6e3	W m^{-2}
$T_0^{(1)}$	1538	°C

$^{(1)}$ from Fig. 2

as in (Amberg, 1991); here, ϵ is chosen as an arbitrarily small parameter. The aforementioned relation to T_l is given by

$$T_l(c_l) = T_0 - \Gamma c_l \tag{12}$$

where T_0 is again the melting temperature of pure iron, and Γ is proportionality constant represented by the slope of the line in the phase diagram in Fig. 2.

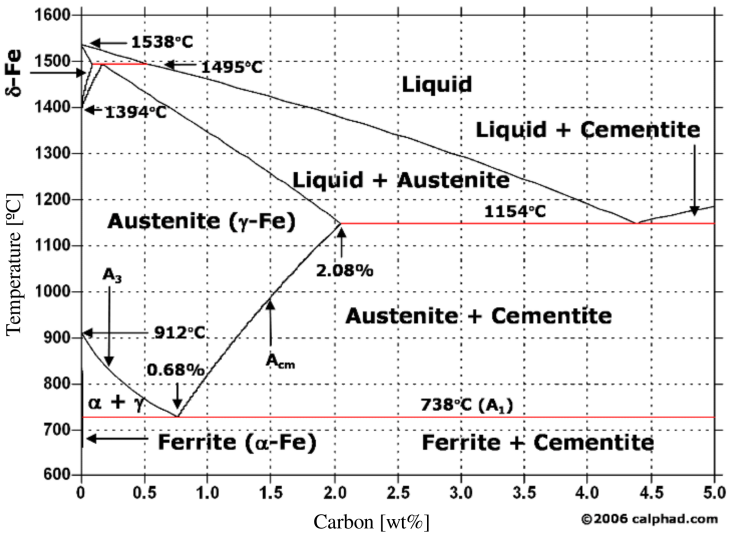

Figure 2: Phase diagram for Fe-C alloy.

3. COMPUTATIONAL IMPLEMENTATION

The methodology applied in the task of solving the previous set of equation, was to make use of Marker and Cell Method (MAC), whose key feature is to proceed to the spatial discretization using a Finite Volume Method over a staggered mesh. The momentum equation is solved by decoupling the velocities and pressure variables by the Projection Method, while the Adams-Bashforth/Crank-Nicolson (ABCN) method to make the temporal numerical integration. The discretization follows the scheme presented in (Prosperetti and Tryggvason, 2007) and (Buscaglia, 2015), with centered

control volumes for each of the variables in the problem - $\mathbf{u}, p, T$ and c_l - as illustrated in Fig. 3.

The numerical methods described above were implemented through an in-house script making use of MATLAB programming environment.

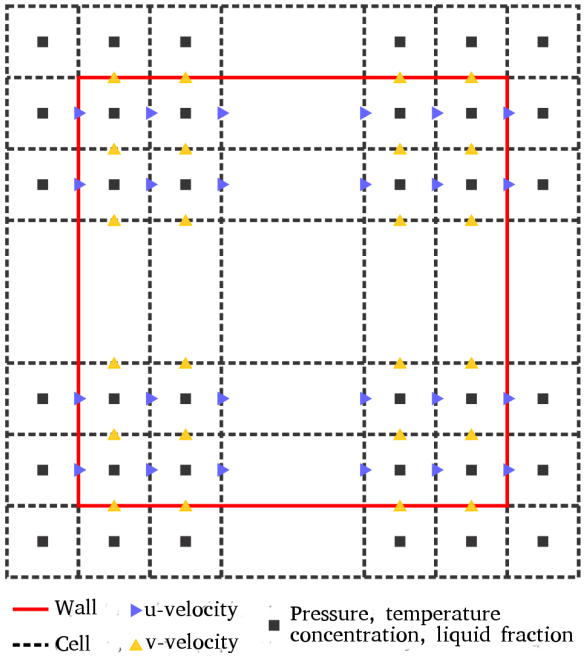

Figure 3: Cell representation for the staggered grid used in the MAC approach. u and v are the x- and y-components of **u,** respectively.

4. RESULTS AND DISCUSSION

The model consisting on the equations presented in Section 2was non-dimensionalized using the following scales

$$[x] = L, \quad [u] = \frac{\alpha}{L}, \quad [t] = \frac{L^2}{\alpha}, \quad [T] = \frac{qL}{\kappa}, \quad [p] = \frac{\rho_0 \alpha^2}{L^2}, \quad [c] = c_0 \tag{13}$$

where $\alpha = \dfrac{\kappa}{\rho C_\mathrm{p}}$, and c_0 is the initial solute concentrations. Replacing the dimensional variables in the original equations and doing the algebra, allows us to identify some classical adimensional numbers used to characterize systems with fluid flow, heat and mass transfer, such as

$$Pr = \frac{\nu}{\alpha}, \quad Ra = \frac{L^3 \beta \Delta T g}{\alpha \nu}, \quad Ga = \frac{L^3 g}{\nu^2}, \quad St = \frac{C_\mathrm{p} \Delta T}{L_\mathrm{at}}, \quad Le = \frac{\alpha}{D} \tag{14}$$

which are known as Prandtl, Rayleigh, Galilei, Stefan, and Lewis number, respectivelly. Applying the relations from Eq. (13), and considering the Eq. (1)-(4) we obtain the non-dimensional equation for momentum

$$\frac{\partial \mathbf{u}^*}{\partial \tau} + \mathbf{u}^* \cdot \overline{\nabla} \mathbf{u}^* - Pr \overline{\nabla}^2 \mathbf{u}^* = -\overline{\nabla} p^* - \frac{L^2}{[H]} Pr \frac{\chi}{H(\chi)} \mathbf{u} + RaPr\, \alpha' \left(T^* - \frac{T_0}{[T]} \right) \mathbf{e}_y + GaPr^2 \left(f c_\mathrm{l} \right) \mathbf{e}_y \tag{15}$$

where the star (*) denotes the variable on its non-dimensional form. Proceding in the same way for the heat transfer, now non-dimensionalizing the Eq. (5), leads to:

$$\frac{\partial T^*}{\partial \tau} + \chi \mathbf{u}^* \cdot \overline{\nabla} T^* = \overline{\nabla}^2 T^* - \frac{1}{\mathrm{St}} \frac{\partial \chi}{\partial \tau} \tag{16}$$

Finally, the non-dimensionalized form of Eq. (8) to model the solute conservation, becomes:

$$\frac{\partial c_\mathrm{m}^*}{\partial \tau} + \mathbf{u}^* \chi \overline{\nabla} c_l^* - \frac{1}{Le} \overline{\nabla}^2 c_l^* = 0 \tag{17}$$

The solution for the non-dimensionalized set of equations and adequate boundary coditions was approximated by computation simulation applying the presented methodology in a domain 20 cm wide and 10 cm high, with insulated top and bottom walls, cooling from the sides at the same given rate q. Thus, horizontal symmetry is assumed and the dependent variables: temperature, pressure, velocities, concentration and liquid fraction are computed for just half of the original domain. The other parameters used in the simulation can be found in Tab. 1. The resulting liquid fraction after 200s of solidification is shown in Fig. 4 with contour lines drawn across the domain.

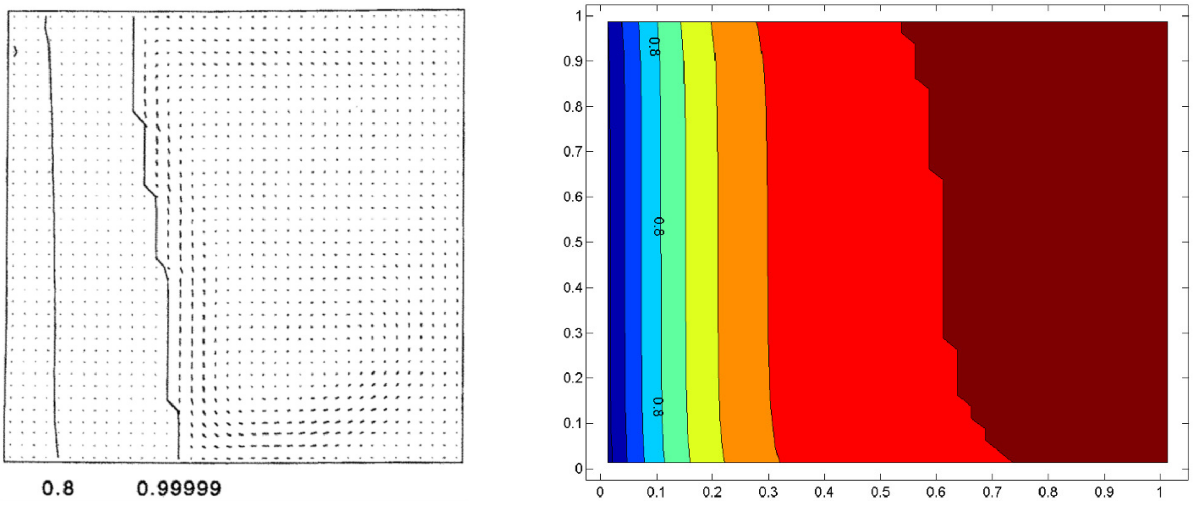

(a) as presented in (Amberg, 1991) (b) obtained by authors

Figure 4: Liquid fraction after 200 s

Figure 5 compares the solute composition of the binary Fe-C alloy after 6000s of solification, both images show relatable differences in concentrations obtained across de domain, with lower concentration at the bottom and higher concentration at the top. Figure 6(a) illustrates the deceleration of velocity field for the region with lower liquid fraction, while Fig. 6(b) shows the corresponding streamlines.

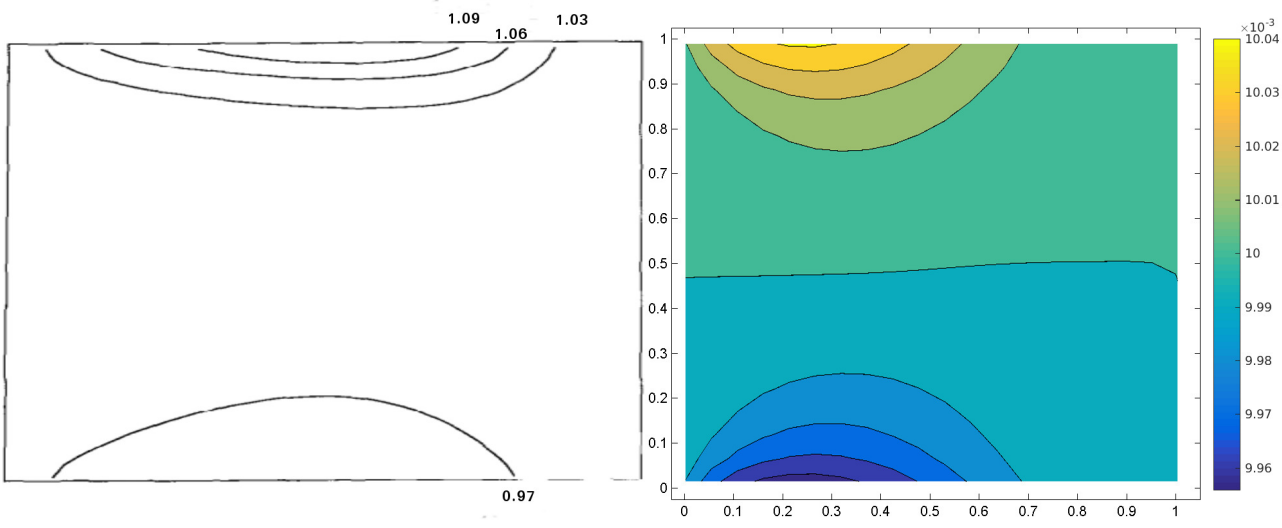

(a) as presented in (Amberg, 1991) (b) obtained by authors

Figure 5: Solute concentration after 6000 s

5. CONCLUSIONS

It can be noticed, that the regions with constant values of liquid fraction are distributed across the domain, in accord with the expected results, while the macrosegregated regions were found in the simulation as in the original paper (Amberg, 1991): greater than average solute concentration in the upper region, and lower than average at the bottom. Besides that, the flow recirculation in the liquid region is in an opposite direction to that in the mushy region, also in accord with theory (Fredriksson and Åkerlind, 2012).

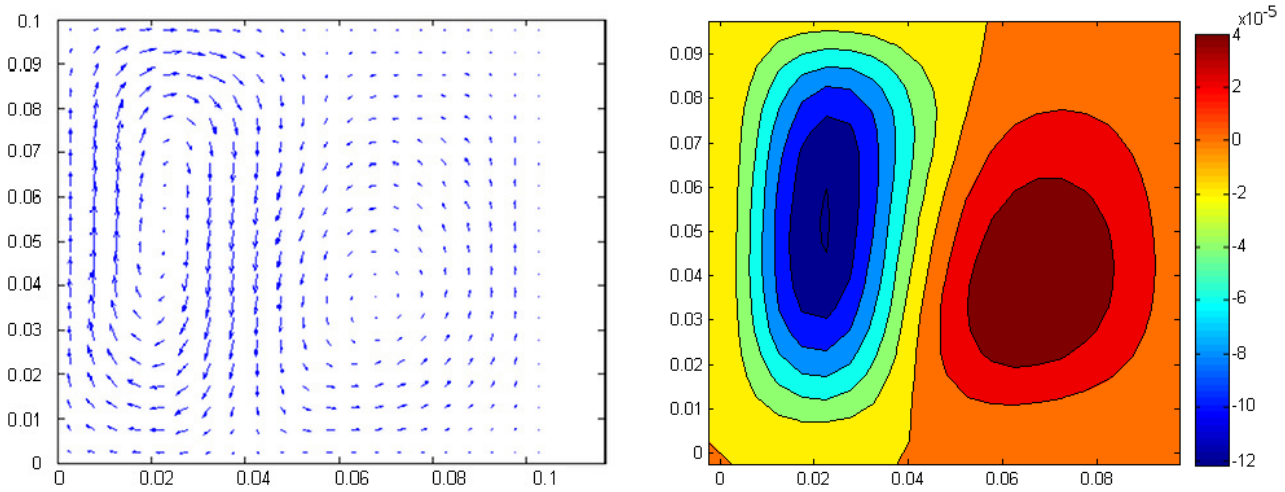

(a) velocity field (b) streamlines obtained from the respective velocity field

Figure 6: Velocity description for the domain half occupied by mush, half occupied by liquid phase, at an early stage of the solidification process

6. ACKNOWLEDGEMENTS

M. Assunção acknowledges the supported provided by FAPESP though the process n.2016/12678-0.

7. REFERENCES

Amberg, G., 1991. "Computation of macrosegregation in an iron-carbon cast". *International Journal of Heat and Mass Transfer*, Vol. 34, pp. 217–227.

Buscaglia, G., 2015. "Notas de aula - sme5802: Introdução à mecânica de fluidos computacional". 1 Oct. 2015 <http://www.lcad.icmc.usp.br/ buscaglia/teaching/>.

Flemings, M., 1974. "Solidification processing". *Materials Science and Engineering Series, McGraw-Hill*.

Fredriksson, H. and Åkerlind, U., 2006. *Materials Processing*. John Wiley and Sons Ltd, 1st edition.

Fredriksson, H. and Åkerlind, U., 2012. *Solidification and Crystallization Processing in Metals and Alloys*. Wiley, New Jersey, 1st edition.

Lienhard IV, J. and Lienhard V, J., 2017. *A Heat Transfer Textbook*. Phlogiston Press, Cambridge, MA, 4th edition. URL `http://ahtt.mit.edu`. Version 2.11.

Maidorn, C. and Blind, D., 1985. "Solidification and segregation in heavy forging ingots". *Nuclear Engineering and Design*, Vol. 84, pp. 285–296.

Olsson, A., 1980. *Department of Casting of Metals*. Ph.D. thesis, Royal Institute of Tecnhology, Stockholm, Sweden.

P. Patil, R. Nalawade, G.B. and Balasubramanian, V., 2015. "Analysis of solidification behaviour of low alloy steel ingot casting - simulation and experimental validation". *Ironmaking and Steelmaking*, Vol. 42, pp. 512–524.

Pickering, E.J., 2013. "Macrosegregation in steel ingots: The applicability of modelling and characterization techniques". *ISIJ International*, Vol. 53, pp. 935–949.

Piwonka, T. and Flemings, M., 1966. "Pore formation in solidification". *Aime Met Soc Trans*, Vol. 236, No. 8, pp. 1157–1165.

Prosperetti, A. and Tryggvason, G., 2007. *Computational Methods for Multiphase Flow Computational Methods for Multiphase Flow*. Cambridge University Press, 1st edition.

West, R., 1985. "On the permeability of the two-phase zone during solidification of alloys". *Metallurgical Transactions A*, Vol. 16A, p. 693.

8. RESPONSIBILITY NOTICE

The authors are the only responsible for the printed material included in this paper.